Jaesool Shim[1]
Prashanta Dutta[1]
Cornelius F. Ivory[2]

[1]School of Mechanical and Materials Engineering, Washington State University, Pullman, WA, USA
[2]School of Chemical Engineering and Bioengineering, Washington State University, Pullman, WA, USA

Received June 30, 2006
Revised August 31, 2006
Accepted September 20, 2006

Research Paper

Modeling and simulation of IEF in 2-D microgeometries

A 2-D finite-volume model is developed to simulate nonlinear IEF in complex microgeometries. This mathematical model is formulated based on the mass conservation and ionic dissociation relations of amphoteric macromolecules, charge conservation, and the electroneutrality condition. Based on the 2-D model, three different separation cases are studied: an IPG in a planar channel, an ampholyte-based pH gradient in a planar channel, and an ampholyte-based pH gradient in a contraction–expansion channel. In the IPG case, cacodylic acid ($pK_1 = 6.21$) and Tris ($pK_1 = 8.3$) are used as the acid and base, respectively, to validate the 2-D IEF model. In the ampholyte-based pH gradient cases, IEF is performed in the pH range, 6.21–8.3 using 10 ampholytes in the planar channel and 20 ampholytes in the contraction–expansion channel. The numerical results reveal different focusing efficiencies and resolution in the narrow and wide sections of the contraction–expansion channel. To explain this, the expressions for separation resolution and peak concentrations of separands in the contraction–expansion channel are presented in terms of the channel shape factor. In a 2-D planar channel, a focused band remains straight all the time. However, in a contraction–expansion channel, initially straight bands take on a crescent profile as they pass through the trapezoidal sections joining the contraction and expansion sections.

Keywords:
Carrier ampholytes / IEF / pH Gradient
DOI 10.1002/elps.200600402

1 Introduction

Electrophoretic transport is defined as the movement of charged solutes in response to an electric field placed across a buffer electrolyte, usually in an anticonvectant medium. Although electrophoresis was introduced 200 years ago [1], it remains popular at laboratory scales due to its extraordinary resolution in a variety of applications. A number of numerical studies have been conducted to elucidate the behavior of electrophoresis in a microchannel [2–6]. These models are generally categorized into four classical modes of electrophoresis: zone electrophoresis (ZE), moving boundary electrophoresis (MBE), ITP, and IEF. MBE, ZE, and ITP create movement of various electrophoretic species along the channel based on their respective electromobilities, whereas IEF allows each ionic component to focus at its stable (fixed) steady-state. In IEF both positively and negatively charged molecules can be separated or concentrated in a pH gradient under the influence of an electric field.

Correspondence: Professor Prashanta Dutta, School of Mechanical and Materials Engineering, Washington State University, Pullman, WA 99164-2920, USA
E-mail: dutta@mail.wsu.edu
Fax: +1-509-335-4662

Abbreviations: CACO, cacodylic acid; **FVM,** finite-volume method; **MBE,** moving boundary electrophoresis

General mathematical descriptions and models of electrophoretic processes were reported in many papers [7, 8]. However, all of the early mathematical models of electrophoresis were established as separate models. In 1981, a universal model of electrophoresis was introduced by Palusinski *et al.* [9] for steady-state processes. Later, Bier *et al.* [10] extended this model to transient problems. The model was designed to predict the behavior of the four classical modes of electrophoresis using chemical equilibrium and physical transport coefficients. Saville *et al.* [11, 12] used this model to simulate MBE and IEF. In their work, histidine was focused in the presence of fixed cacodylic acid (CACO) and Tris gradients in a 1-D geometry. In a research monograph, Mosher *et al.* [5] reported their method of handling weak and strong acids and bases, ampholytes, and proteins. For IEF in the presence of many ampholytes, Mao *et al.* [4] modeled the dynamics of CIEF without fluid flow using a 1-D geometry with 150 ampholytes to cover the pH range ~3–10. Arnaud *et al.* [6] simulated off-gel buffering, *i.e.*, neutralization of ampholytes in a solution before penetrating the gel, using the finite-element method (FEM). Chatterjee [3] developed generalized numerical formulations using the finite-volume method (FVM) to simulate a complex 3-D geometry. In that work, a scalable computational model was developed for microfluidic applications, but he simulated only IEF using an immobilized CACO-histidine gradient. More recently, Thormann *et al.* [2] compared simulation data obtained from

a 1-D IEF model, and their results (qualitatively) agree well with experimental results obtained from whole column optical imaging.

A 1-D model is not sufficient if one desires to observe the behavior of proteins during separation in complex microgeometries. Both ampholytes and proteins have different transient behavior in the complex geometry. The transient behavior of proteins in the presence of many carrier ampholytes has not been reported in complex geometries until now. In this study, a generalized 2-D (spatial) IEF model is developed to study geometric effects on the transient focusing behavior of simulated ampholytes with small ΔpKs and ersatz "proteins" with only three charged states surrounding a pI. The small ampholyte ΔpKs, although they provide an optimistic estimate of system performance compared with commercial ampholytes, are sufficient to demonstrate that the simulation is working properly. The small number of charged states assigned to our separands has the end-result of providing a poor approximation to a protein at short times when these components are far away from their pIs, but a reasonably good approximation to focusing behavior in the neighborhood of their focused steady state. Both of these limitations are relatively easy to modify in the code and will be adjusted in future simulations.

To verify the 2-D IEF model, we compared our results of IPG with an existing 1-D IEF model [12]. In addition, simulations were performed for ampholyte-based IEF in 2-D planar (Fig. 1a) and contraction–expansion channels (Fig 1b). For the IEF simulation in a planar channel, ten ampholytes and one protein are used, while in the contraction–expansion channel, 20 ampholytes and 4 proteins are considered. The 2-D simulation results in the complex channel are then compared to those in a simple planar channel. To our knowledge, this is the first numerical study on 2-D IEF (ampholyte-based pH gradient) where contraction–expansion geometry is used to explore the transient behavior of proteins and ampholytes.

The remainder of this paper is organized as follows: in Section 2, a mathematical model is presented for IEF along with relevant assumptions. In Section 3, the resolution and peak (concentrations) heights of proteins are introduced for a contraction–expansion channel. In Section 4, the numerical scheme is presented. In Section 5, we show the numerical results and discussion of 2-D IEF in planar and contraction–expansion microchannels. The conclusions are presented in Section 6.

2 IEF model

IEF is a powerful separation technique used in proteomics to concentrate and isolate proteins based on their pI [13]. An electromagnetokinetic theory of IEF was introduced by Leenov and Kolin [14] by calculating the electrophoretic

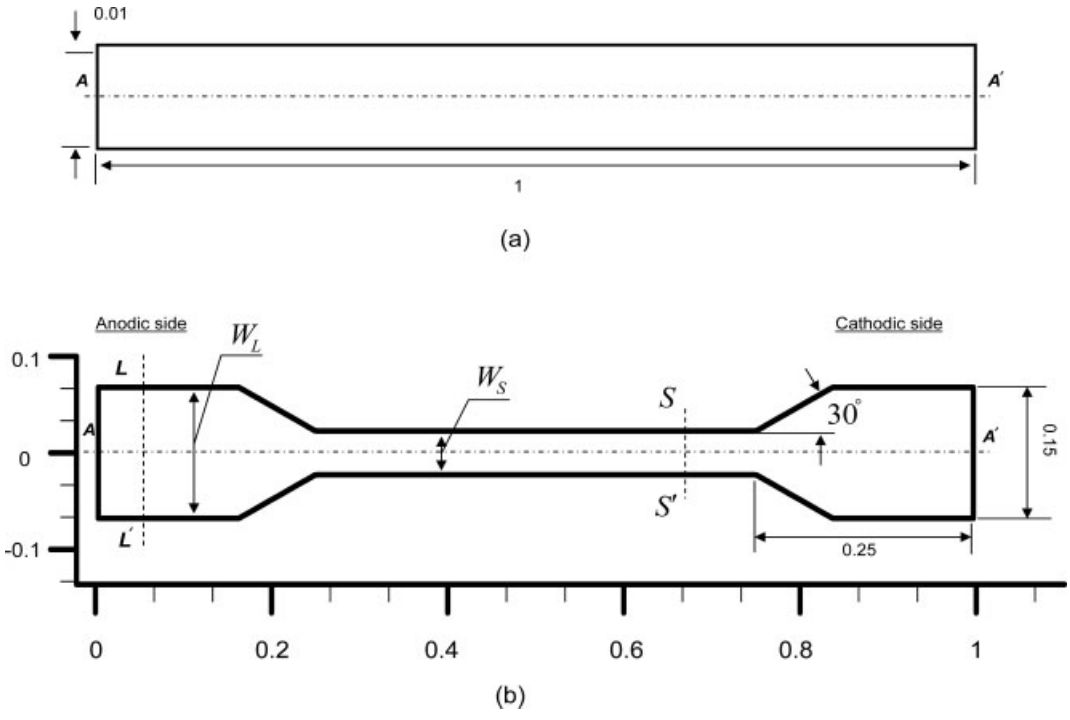

Figure 1. Schematic diagram of (a) a 2-D planar channel (1 cm × 100 μm) used to simulate the IPG case and ampholyte-based pH gradient case. (b) Schematic of a 3:1:3 oblique contraction–expansion channel used for ampholyte-based pH gradient IEF. The anode and cathode are placed at the left and right sides of these channels. All channel dimensions are presented in terms of centimeters. Figures are not to scale.

forces on spherical and cylindrical particles analytically. This group first created a stable pH gradient using two chemical buffers [15], and this work catalyzed subsequent research on the development of a pH gradient using carrier ampholytes. In 1961, Svensson presented a theoretical work on "natural pH gradients", and showed that a stable pH gradient can be established and maintained in the presence of carrier ampholytes (a mixture of low-molecular-weight ampholytes) [16]. On-chip IEF is currently receiving significant attention due to its shorter processing time, high resolution, low reagent consumption, and overall cost effectiveness [17–18]. In order to make the most of these advantages, a 2-D model is needed as an aid in platform design and protocol development.

Ampholyte-based IEF takes place in a soup of partially ionized solutes whose charge characteristics are determined by a set of dissociation reactions. The following derivation is a minor departure from the generalized vector treatment of Mosher *et al.* [5] in which we treat each component, C_i, as being composed of a set of species, S_{ij}, which are summed over j to recover each of the i components in our system, *i.e.*,

$$C_i = \sum_{j=1}^{J_i+1} S_{ij} \tag{1}$$

This allows us to treat all weak acids and bases, ampholytes, proteins, and even water, which dissociates into hydronium and hydroxide ions, as being mathematically equivalent. The mean charge, $\langle z_i \rangle$, on component, C_i, is then defined by summing over the charges on the species that make up that component, *e.g.*,

$$\langle z_i \rangle C_i = \sum_{j=1}^{J_i+1} z_{ij} S_{ij} \tag{2}$$

The basic "mass–action" relationship between charge-adjacent species of the same component is

$$S_{ij+1} + H_2O = S_{ij} + H_3O^+ \tag{3}$$

S_{i1} is the most electronegative species and S_{iJ_i+1} is the most positive with a total of J_i dissociable groups. This relation can be expressed in the form of a kinetic equation,

$$\Lambda_{ij} = k_{ij}^r (K_{ij} S_{ij+1} - H_3O^+ S_{ij}) \tag{4}$$

where the high concentration of water has been subsumed into the equilibrium coefficient, K_{ij}, and k_{ij}^r is a reverse-reaction kinetic coefficient which is assumed to be large. The molar flux, $\vec{\mathbf{N}}_{ij}$, of each species is

$$\vec{\mathbf{N}}_{ij} = -D_{ij} \nabla S_{ij} + (\vec{\mathbf{U}} + z_{ij} \omega_{ij} \vec{\mathbf{E}}) S_{ij} \tag{5}$$

where D_{ij} is the species diffusion coefficient, ω_{ij} is the absolute mobility, $\vec{\mathbf{E}}$ is the electric field, and $\vec{\mathbf{U}}$ is the bulk velocity of the buffer. The mass conservation equation for each species may be written as

$$\begin{aligned}
&\frac{\partial}{\partial t} S_{i1} + \nabla \cdot \vec{\mathbf{N}}_{i1} = \Lambda_{i1} \quad \text{if } j = 1 \\
&\frac{\partial}{\partial t} S_{ij} + \nabla \cdot \vec{\mathbf{N}}_{ij} = \Lambda_{ij} - \Lambda_{ij-1} \quad \text{if } 1 < j < J_i + 1 \\
&\frac{\partial}{\partial t} S_{iJ_i+1} + \nabla \cdot \vec{\mathbf{N}}_{iJ_i+1} = -\Lambda_{iJ_i} \quad \text{if } j = J_i + 1
\end{aligned} \tag{6}$$

where the terms on the right-hand side of Eq. (6) account for the generation and consumption of S_{ij}. Summing the conservation equations for the $J_i + 1$ species yields

$$\frac{\partial}{\partial t} C_i + \nabla \cdot \vec{\mathbf{N}}_i = \sum_{j=1}^{J_i+1} (\Lambda_{ij} - \Lambda_{ij-1}) = 0 \tag{7}$$

where $\vec{\mathbf{N}}_i = \sum_{j=1}^{J_i+1} \vec{\mathbf{N}}_{ij}$ and, if all $D_{ij} = D_i$ and $\omega_{ij} = \omega_i$, Eq. (7) becomes

$$\frac{\partial}{\partial t} C_i - \nabla \cdot (D_i \nabla C_i) + \nabla \cdot (\vec{\mathbf{U}} C_i) + \nabla \cdot (\omega_i \vec{\mathbf{E}}) \sum_{j=1}^{J_i+1} (z_{ij} S_{ij}) = 0 \tag{8}$$

Then using Eq. (2), we obtain

$$\frac{\partial}{\partial t} C_i + \nabla \cdot \left[\left(\vec{\mathbf{U}} + \langle z_i \rangle \omega_i \vec{\mathbf{E}} \right) C_i - D_i \nabla C_i \right] = 0 \tag{9}$$

which provides a single partial differential equation for each component. If the dissociation reactions are fast, we also have J_i algebraic relations among the component i species,

$$K_{ij} = \frac{H_3O^+ S_{ij}}{S_{ij+1}} \tag{10}$$

which must be solved together with Eq. (9) for each component. The relations between components and their associated species are

$$\begin{aligned}
C_i &= S_{ij} \left(1 + \sum_{jj=1}^{J_i} \prod_{k=1}^{jj} \frac{H_3O^+}{K_{ik}} \right) \quad \text{if } j = 1, \\
C_i &= S_{ij} \left(\prod_{k=1}^{j-1} \frac{K_{ik}}{H_3O^+} \right) \left(1 + \sum_{jj=1}^{J_i} \prod_{k=1}^{jj} \frac{H_3O^+}{K_{ik}} \right) \quad \text{if } j \geq 2
\end{aligned} \tag{11}$$

2.1 Charge density and current density

We define the current density $\vec{I}$ and the charge density ρ as

$$\begin{aligned}
\vec{\mathbf{I}} &= F \sum_{i=1}^{I} \left(\sum_{j=1}^{J_i+1} z_{ij} \vec{\mathbf{N}}_{ij} \right) \\
&= F \sum_{i=1}^{I} (-D_i \nabla (\langle z_i \rangle C_i) + \langle z_i \rangle \vec{\mathbf{U}} C_i + \langle z_i^2 \rangle \omega_i \vec{\mathbf{E}} C_i)
\end{aligned} \tag{12}$$

$$\rho = F \sum_{i=1}^{I} \left(\sum_{j=1}^{J_i+1} z_{ij} S_{ij} \right) = F \sum_{i=1}^{I} \langle z_i \rangle C_i \tag{13}$$

where $\langle z_i^2 \rangle C_i = \sum_{j=1}^{J_i+1} z_{ij}^2 S_{ij}$, F is the Faraday constant, and I is the number of components which include H_3O^+ and OH^- ions as $(I-1)$th and Ith components. Noting that the charge density, $\rho \approx 0$, we obtain the electroneutrality constraint as

$$\rho = F\sum_{i=1}^{I}\langle z_i\rangle C_i = 0 \tag{14}$$

The reader should note that $\langle z_i\rangle$ is a function of time and position while z_{ij} is not.

2.2 Hydronium ion

Hydronium is unusual among all the ionic species in our system in that it participates in every dissociation reaction that produces or consumes a proton, including the dissociation of water to create a hydroxyl ion and a hydronium ion. In this study, hydroxyl and hydronium ions are denoted by subscripts OH and H. Now, assuming no bulk flow ($\vec{\mathbf{U}} = 0$), the mass conservation equations for these two ions are

$$\frac{\partial}{\partial t}C_H + \nabla\cdot z_H\omega_H\vec{\mathbf{E}}\,C_H - D_H\nabla^2 C_H = -\Lambda_{H_2O} + \sum_{i=1}^{I-2}\sum_{j=1}^{J_i}\Lambda_{ij} \tag{15}$$

$$\frac{\partial}{\partial t}C_{OH} + \nabla\cdot z_{OH}\omega_{OH}\vec{\mathbf{E}}\,C_{OH} - D_{OH}\nabla^2 C_{OH} = -\Lambda_{H_2O} \tag{16}$$

with the equilibrium relation.

$$K_W = C_{OH}C_H \tag{17}$$

where Λ_{H_2O} is the reaction term with hydroxyl ion to form water and K_w is the equilibrium constant. These two equations (Eqs. 15 and 16) may be subtracted from one another to eliminate Λ_{H_2O}, and the equilibrium relation is used to eliminate C_{OH} to get

$$\frac{\partial}{\partial t}\left(C_H - \frac{K_W}{C_H}\right) + \nabla\cdot\left(\mu_H C_H - \mu_{OH}\frac{K_W}{C_H}\right)\vec{\mathbf{E}} = \nabla^2\left(D_H C_H - D_{OH}\frac{K_W}{C_H}\right) + \sum_{i=1}^{I-2}\sum_{j=1}^{J_i} j\left(\frac{\partial}{\partial t}S_{ij} + \nabla\cdot\mu_{ij}\vec{\mathbf{E}}\,S_{ij} - D_{ij}\nabla^2 S_{ij}\right) \tag{18}$$

where the summation is over all dissociation reactions except the hydrolysis reactions, and $\mu_{ij} = z_{ij}\omega_{ij}$.

Note that the algebraic electroneutrality condition allows us to eliminate one differential conservation equation from the set which needs to be solved numerically; it is convenient to choose to eliminate Eq. (18) for hydronium because it is so complex.

2.3 Model equation

The set of equations which must be simultaneously solved consists of one conservation Eq. (9) for each component in our system except hydronium (and hydroxyl), an electroneutrality condition of the form

$$C_H - \frac{K_W}{C_H} = -\sum_{i=1}^{I-2}\langle z_i\rangle C_i \tag{19}$$

which allows us to solve for hydronium (and hydroxyl) ion concentrations and an equation for the electric potential based on the true current

$$\nabla\cdot(\sigma\vec{\mathbf{E}}) = \sum_{i=1}^{I}\sum_{j=1}^{J_i+1} z_{ij}D_{ij}\nabla\cdot\nabla S_{ij}$$

$$\text{where } \sigma = F\sum_{i=1}^{I}\sum_{j=1}^{J_i+1} z_{ij}^2\omega_{ij}S_{ij} \tag{20}$$

This leaves us with component equations, an electroneutrality equation, the hydrolysis Eq. (17) and charge (current) conservation Eq. (20) which must be solved simultaneously for unknowns including all components plus the electric potential.

In all previous derivations of the model equations for IEF, it has been assumed that the current density is the same at every point in the model domain, a 1-D channel, so Eq. (12) could be used to calculate the local electric field and the electrode voltage. However, when this model is extended to two or more spatial dimensions, the assumption of uniform current must be relaxed and spatial variations in the electric field must be calculated using the full set of transport equations for all species including dissociation equilibrium relations, the current conservation equation, and an electroneutrality condition.

2.4 Computational model

In our computational model, the concentrations of amphoteric molecules are obtained from the component transport (mass conservation) equations. During separation, all ionic components, including water, are in chemical equilibrium which implies that the ionic reactions are fast enough that the individual components remain in a pseudoequilibrium state. In this study, we assumed that each of the ampholytes and proteins have three charge states so that only the two dissociation constants near their p*I*s have a significant effect on the transient behavior of the carrier ampholytes and proteins whose mean charge is given by Eq. (2). This model neglects heat generation due to Joule heating effects, *i.e.*, temperature is assumed constant throughout the channel. Electrokinetic flow is not considered here since the IEF channel is coated with methylcellulose to suppress electroosmosis [17–18]. For the species that make up a particular component, the absolute mobilities and diffusivities of all charge states are assumed to be the same. Moreover, we have not considered corrections to activity coefficients and mobilities of electrolytes [19] and polyelectrolytes [20].

The concentration of hydronium is calculated from the electroneutrality equation, while the hydroxyl concentration is obtained from Eq. (17). The electric potential (ϕ) is calculated from the charge conservation equation using the mean square valence for all proteins and ampholytes. The Nernst–Einstein equation $\left(D_i = \frac{RT\omega_i}{F}\right)$ is used to calculate the diffusion coefficient from the absolute mobility [11], where R is the gas constant and T is the absolute temperature.

The boundary conditions for the mass conservation equations consist of imposition of zero net flux ($N_i = 0$) at the anolyte and catholyte reservoirs and no penetration on the channel surfaces. The charge conservation equation is solved based on insulating boundary conditions ($\nabla\phi \cdot \vec{\mathbf{n}} = 0$) on the channel surfaces and constant electric potentials at the anolyte and catholyte reservoirs. The insulating boundary condition at the channel wall is justified because silicon, glass, PDMS, or some other insulating material is typically used as microchannel wall.

Three cases are studied using the above-mentioned IEF model: an IPG IEF within simple 2-D planar geometry, ampholyte-based IEF in a simple, 2-D planar geometry (Fig. 1a), and ampholyte-based IEF in a complex 2-D geometry (Fig. 1b). For the IPG, linear concentration distributions of an acid and a base are used to form the IPG. In this case, the mobilities of acid and base are set to zero, and the amphoteric molecules migrate to their p*Is via* electromigration and diffusion. On the other hand, an ampholyte-based pH gradient is formed by interactions between ampholytes and electric fields. For a 2-D planar microchannel, an ampholyte-based pH gradient is produced in the presence of 10 ampholytes, while 20 ampholytes are used in case of 2-D contraction–expansion channel.

3 IEF resolution in a contraction–expansion channel

In this section, an analysis is presented for the expected SD, peak concentration, and resolution in a contraction–expansion channel based on an idealized model for IEF [21]. Consider a straight channel with a linear pH gradient and a constant conductivity in which several proteins have focused to their steady-state profiles. Since the net flux of a stationary, focused band is zero, it can be written in terms of a constant electric field as

$$N_i(x) = -D_i\frac{\partial C_i(x)}{\partial x} - (x - x_f)\omega_i\left|\frac{\partial(\mathrm{pH})}{\partial x}\frac{\mathrm{d}\langle z_i\rangle}{\mathrm{d}(\mathrm{pH})}E_x\right|C_i(x) = 0 \tag{21}$$

where x_f is the focal point of the protein. The focal point is the position along the *x*-axis where the pH of the ampholyte solution is equal to the p*I* of the protein, *i.e.*, the point at which $\langle z_i\rangle = 0$. The concentration profile of the focused protein is obtained by integrating Eq. (21) to get

$$c_i(x) = A\,\exp\left[-\alpha\frac{(x - x_f)^2}{2}\right]$$

$$\text{where } \alpha = \left(\left|\frac{\mathrm{d}\langle z_i\rangle}{\mathrm{d}(\mathrm{pH})}\frac{\partial(\mathrm{pH})}{\partial x}\,E_x\right|\right)\frac{\omega_i}{D_i} \tag{22}$$

and *A* is an integration constant. The SD of a protein band about its focal point can be calculated from Eq. (22) using moment analysis to obtain

$$\sigma_i = \sqrt{\frac{D_i}{\left|\frac{\mathrm{d}\langle z_i\rangle}{\mathrm{d}(\mathrm{pH})}\frac{\partial(\mathrm{pH})}{\partial x}E_x\right|\omega_i}} \tag{23}$$

Using Eq. (23) and the Nernst–Einstein equation, the separation resolution in a 2-D straight channel can be written as

$$R = \frac{|x_{f,1} - x_{f,2}|}{4\sigma} \cong \left(\frac{\Delta pI}{4}\right)\sqrt{\frac{E_xF}{RT}\left|\frac{\frac{\mathrm{d}}{\mathrm{d}(\mathrm{pH})}(\langle z_i\rangle)}{\frac{\partial}{\partial x}(\mathrm{pH})}\right|} \tag{24}$$

Let us consider what happens to a focused band as it passes from a large channel with width, W_L, into a smaller channel with width, W_S, experiencing a reduction in channel width by a factor of

$$f_w = \frac{W_L}{W_S} \tag{25}$$

Keeping in mind that the mass of protein in both positions is the same and assuming that the proteins are present in vanishingly small amounts, they will be tightly focused into the Gaussian peaks predicted by the idealized theory immediately above. Further approximating the concentration profiles of the protein in each section as triangles, we can write the following formula for the mass (*M*) at each position:

$$M_L = \frac{(4\sigma_L)W_LC_LH_L}{2} = \frac{(4\sigma_S)W_SC_SH_S}{2} = M_S \tag{26}$$

where *H* is the channel height. The subscripts S and L correspond to the small (section $S - S'$) and large (section $L - L'$) cross-sectional regions as shown in Fig. 1b.

Noting that the channel height is constant, *i.e.*, $H_L = H_S$, solving Eq. (26) for the ratio of the concentrations and using Eq. (23) to replace the SD yields

$$\frac{C_S}{C_L} = \frac{\sigma_LW_LH_L}{\sigma_SW_SH_S} = \frac{\sigma_L}{\sigma_S}f_w = f_w\sqrt{\frac{\left.\frac{\mathrm{d}(\mathrm{pH})}{\mathrm{d}x}\right|_S E_{x,S}}{\left.\frac{\mathrm{d}(\mathrm{pH})}{\mathrm{d}x}\right|_L E_{x,L}}} \tag{27}$$

Under ideal conditions, the change in the local electric field and pH gradient between these two locations can be expressed as

$$E_{x,S} = f_wE_{x,L} \tag{28}$$

$$\left.\frac{\partial(\mathrm{pH})}{\partial x}\right|_S = \frac{1}{f_w}\left.\frac{\partial(\mathrm{pH})}{\partial x}\right|_L \tag{29}$$

so the increase in concentration as a band moves into the narrow channel is f_w.

Furthermore, using Eq. (24), the ratio of the resolutions in the small and large sections can be found as

$$\frac{R_S}{R_L} = \frac{\left(\frac{\Delta pI}{4}\right)\sqrt{\frac{E_{x,S}F}{RT}\frac{\frac{\mathrm{d}}{\mathrm{dpH}}\langle z_i\rangle}{\left(\frac{\partial}{\partial x}\mathrm{pH}\right)_S}}}{\left(\frac{\Delta pI}{4}\right)\sqrt{\frac{E_{x,L}F}{RT}\frac{\frac{\mathrm{d}}{\mathrm{dpH}}\langle z_i\rangle}{\left(\frac{\partial}{\partial x}\mathrm{pH}\right)_L}}} = \sqrt{\frac{E_{x,S}}{E_{x,L}}}\sqrt{\frac{\left(\frac{\partial}{\partial x}\mathrm{pH}\right)_L}{\left(\frac{\partial}{\partial x}\mathrm{pH}\right)_S}} = f_w \tag{30}$$

where R_L and R_S are the resolutions of proteins in large and small sections of the channel, respectively.

4 Numerical scheme

A variety of computer simulations of IEF have been studied using only a 1-D IEF model because the calculations are very complicated and time consuming. The most common consideration involves how one treats amphoteric molecules such as proteins and carrier ampholytes in a discretized fashion in a computer simulation. In this work, 2-D FVM is developed to solve the transport equations with electromigration and diffusion given by Eq. (9) together with the charge conservation equation defined in Eq. (20). Since the mathematical model of IEF is highly nonlinear, structured grids are considered for the sake of computational simplicity and stability. The discretized algebraic equations are derived at each grid point for mass and charge conservation equations. The power law scheme is used to form coefficients of algebraic equations [22]. For advection-diffusion problems, this scheme provides better accuracy at reasonable time. The tridiagonal matrix algorithm (TDMA) is used to solve the discretized algebraic equations along a grid line, and the line by line iteration is employed until conserved results are obtained throughout the computational domain. In the case of the electroneutrality equation, the Newton–Raphson method is used to obtain the concentration of hydronium ions. In our simulation, the convergence criteria are 10^{-4} for mass conservation and 10^{-5} for charge conservation and chemical electroneutrality. In order to obtain the grid-independent results, 3000 grid points are used for straight channel cases, while 8000 elements are used (400 grids in the length and 20 grids in the width) for the contraction–expansion geometry. The simulations are performed on an XP-based Dell computer (Pentium (R) 4 Cpu, 3.4 GHz, and 2 GB RAM). For the IPG case, the program took approximately 12 days, while the computational times were 30 and 54 days for ampholyte-based pH gradient cases in straight and expansion-contraction channels, respectively.

5 Results and discussion

Several numerical simulations are performed to demonstrate the transient behavior of amphoteric molecules in a multidimensional electric field. In particular, they illustrate how a homogeneous mixture of ampholytes rearrange themselves as they approach steady state in a 2-D channel under an applied electric potential. This redistribution of ampholytes provides a stable pH gradient which allows the proteins to focus at their p*I*s. Two different pH methods are considered in this study: an IPG and an ampholyte-based pH gradient. Moreover, two different geometries, a 2-D planar channel and a 2-D contraction–expansion channel, are used for the IEF simulation. The effect of the applied electric potential on the focusing speed of the target components is noted as well.

5.1 IEF by IPG

To verify the 2-D model, an IPG IEF is simulated. The input parameters were taken from the literature [11, 12] except that a constant electric potential difference was applied across the channel rather than a constant current. Many 1-D IEF models have assumed a constant current in the domain, but a constant current is not normally used in practice. The input data for this case are listed in Table 1. A pH range of 6.21–8.3 is formed using CACO and Tris. In this simulation, the mobilities of CACO and Tris are set to zero, essentially fixing a pH gradient in place. The initial concentration of histidine is uniformly mixed and distributed over the entire channel, but the concentration lines of CACO and Tris are intersected with each other as shown in Fig. 2. The amount of histidine in comparison to that of CACO and Tris is very small (less than 5%). The electric potential at the anode is varied from case to case, while the electric potential at the cathode is ground for a 1 cm long and 100 μm-wide channel (see Fig. 1a).

The evolution of the histidine concentration profile is shown in Fig. 3a for a nominal electric field of 40 V/cm. The concentration of histidine near the center of the channel increases from its initial value (1 mM), while its concentration at the anodic and cathodic sides decreases because the p*I* of histidine is located close to the channel center (~0.6 cm in Fig. 3a). During the IEF process, the concentration profile of histidine changes from an early asymmetrical shape to a symmetric form. At steady state, the concentration profile becomes nearly Gaussian. In this simulation, the steady state is achieved within 60 min of the initiation of IEF.

The transient behavior of electrical conductivity in the channel is shown in Fig. 3b and reflects the fact that only mobile, charged species contribute to the current. At the start of focusing, the conductivity at the electrodes is higher than at the center mainly due to the increased charge on the histidine at pH values above and below its p*I* but it quickly decreases at the edges of the channel as the histidine clears away from the edges of the channel. During the focusing process, the conductivity in the center region increases with the histidine concentration (Fig. 3b) implying that the concentration of histidine has a crucial effect on the conductivity. Note that, although the net flux of histidine is zero, the interequilibrating, charged species that sum to make up the histidine component have nonzero concentrations and therefore contribute to the conductivity and the current passing through histidine's p*I*.

Figure 3c shows the IPG developed in the system due to the presence of CACO, Tris, and histidine. Numerical results show that the pH profiles remain almost the same during this focusing process. The numerical results obtained from our 2-D model are similar to those of Palusinski *et al.* [12], except that, in their case they modeled a 1-D constant channel.

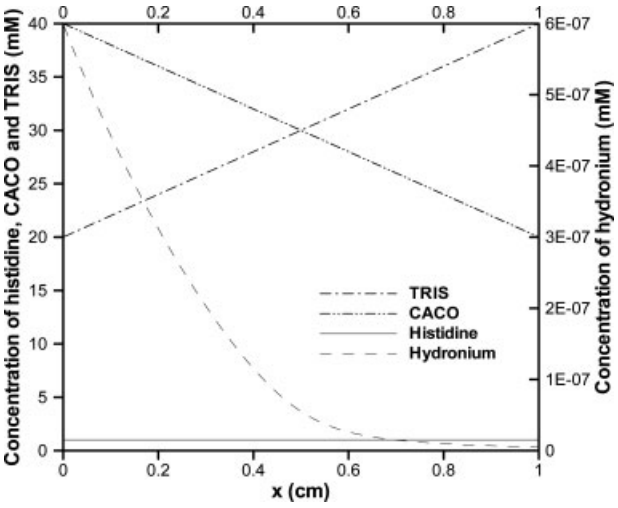

Figure 2. Initial concentration distributions of CACO, Tris, histidine, and hydronium for IPG case.

Table 1. Input properties of acid, base, and histidine used for IEF simulation

Component	pK_1	pK_2	pI	Concentration (mol/m^3)	Mobility (m^2/V·s)
CACO	6.21			40–20	0
Tris	8.3			20–40	0
Histidine	6.04	9.17	7.61	1	2.02E-08

Histidine is considered as three charged states. Diffusion coefficient is calculated using the Nernst–Einstein equation. CACO and Tris are used as the acid and base, respectively.

The effects of the applied electric potential on focusing speed were also investigated. Three different electric potentials (30, 40, and 50 V) are used at the anode, while the cathode is connected to a ground (0 V). At higher electric potentials, histidine focuses faster. For example, at 50 V, the steady state is achieved in 2000 s, while it took 3600 s for the 40 V case. The bandwidths (4σ) of focused proteins are calculated (using moment analysis) as 0.479, 0.443, and 0.417 cm for nominal electric fields of 30, 40, and 50 V/cm, respectively. Thus, for a particular geometry, the band width of the focused protein linearly decreases with the electric potential (Fig. 4).

5.2 IEF by ampholyte-based pH gradient in a straight channel

An ampholyte-based pH gradient and an IPG are different mainly with respect to the formation of the pH profile. The former is made by interactions between ampholytes under the influence of an applied current, while the latter is formed by the immobilization of acidic and/or basic moieties in a porous phase, *e.g.*, gel, with narrow pores.

For the planar microchannel shown in Fig. 1a, a monotonic pH gradient is simulated using ten ampholytes whose physicochemical characteristics are summarized in Table 2. Here, the ΔpIs of the ampholytes are uniform and one "protein" with pI = 7.3 midway between widely spaced pKs is allowed to focus in the pH range of 6.21–8.3. The potential at the cathode is set at 0 V (ground), while the potential at the anode is fixed at either 100 or 300 V. It is assumed that all ampholytes and proteins are uniformly mixed and distributed along the channel at the beginning of the separation process. The initial concentration of each ampholyte is ten times higher than that of the protein and all ampholytes and proteins are treated as having three charged states.

Figure 5 shows the focusing of proteins and ampholytes at various times during the autoformation of the ampholyte-based pH gradient. During the transient period, most of the ampholytes initially form pairs of peaks on the anodic and cathodic edges of the channel (Fig. 5a), which move toward the channel center (Fig. 5c). However, ampholytes with pIs (pI = 6.21, 6.45, 8.07, 8.3) produce only a single peak (Figs. 5a and b) as they approach the steady state. Unlike the IPG case, the pH gradient changes until IEF reaches steady state as shown in Fig. 6. Note that a very steep pH gradient is initially formed at each electrode with no pH gradient in the center of the channel. The pH gradient gradually forms as focusing proceeds and, eventually, the pH distribution takes on a step-like shape. In practice, a stepwise pH profile is not unusual in a simulation where only ten ampholytes are used [5]. Some studies have reported the stepwise pH phenomenon during IEF simulations [5, 20]. To avoid this, Svensson [23] proposed an equation by introducing certain factors into his mathematical model including the number of ampholytes *per* pH unit, the ΔpI of the ampholytes, and the acidic and basic equilibrium constants [23]. In our numerical simula-

Table 2. Input properties of ten ampholytes and one protein used for IEF simulation in a 2-D planar channel

Component	pK_1	pK_2	pI	Concentration (mol/m^3)	Mobility (m^2/V·s)
Ampholyte 1	6.01	6.41	6.21	0.16	3.0E-08
Ampholyte 2	6.25	6.65	6.45	0.16	3.0E-08
Ampholyte 3	6.47	6.87	6.87	0.16	3.0E-08
Ampholyte 4	6.71	7.11	6.91	0.16	3.0E-08
Ampholyte 5	6.94	7.34	7.14	0.16	3.0E-08
Ampholyte 6	7.17	7.57	7.37	0.16	3.0E-08
Ampholyte 7	7.51	7.91	7.71	0.16	3.0E-08
Ampholyte 8	7.64	8.04	7.84	0.16	3.0E-08
Ampholyte 9	7.87	8.27	8.07	0.16	3.0E-08
Ampholyte 10	8.10	8.50	8.30	0.16	3.0E-08
Protein 1	7.00	7.60	7.30	0.016	3.0E-08

All the ampholytes and the protein are regarded as three charged states of analytes for simulation. All initial concentrations are uniformly mixed and distributed over the entire channel.

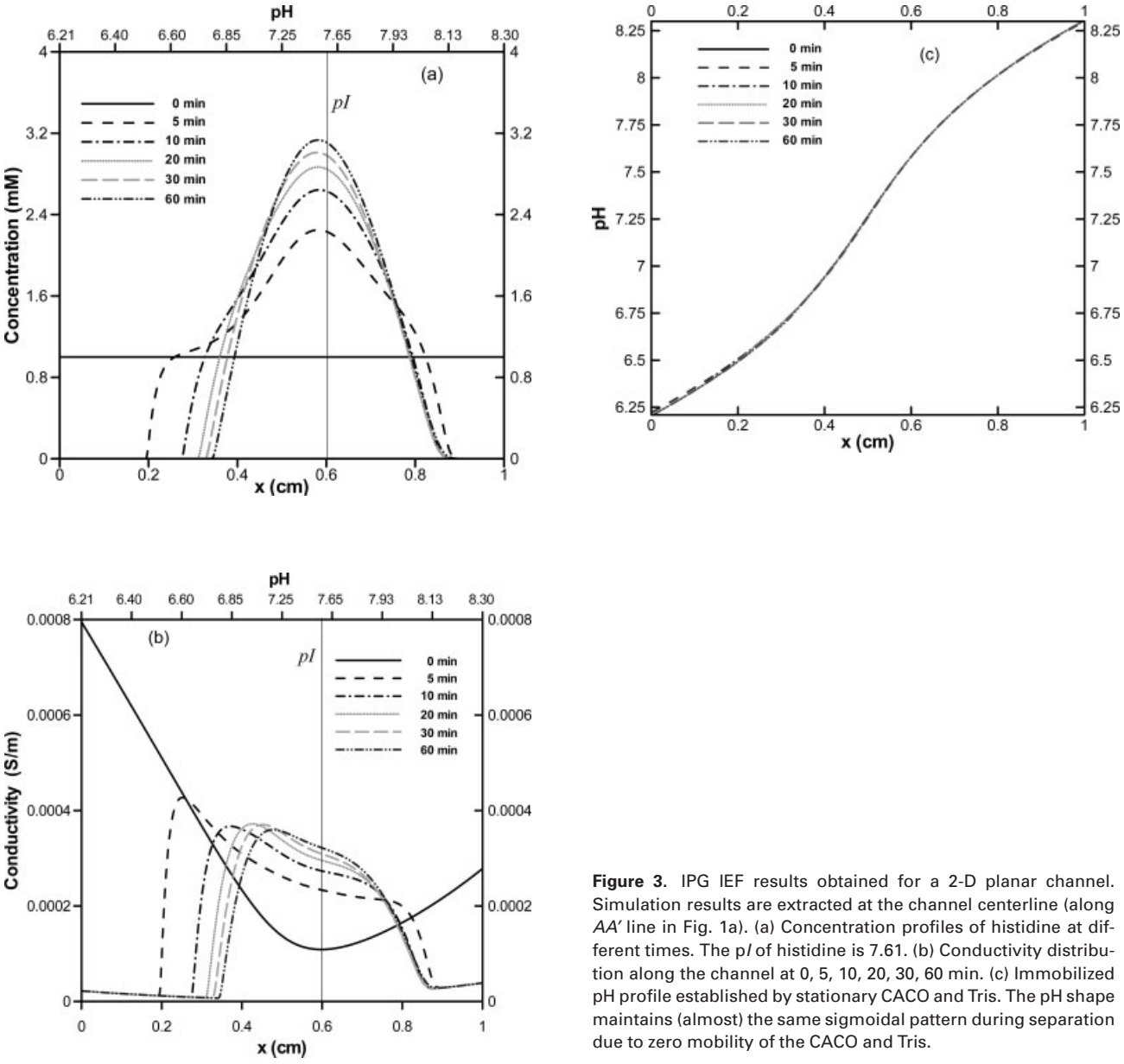

Figure 3. IPG IEF results obtained for a 2-D planar channel. Simulation results are extracted at the channel centerline (along *AA′* line in Fig. 1a). (a) Concentration profiles of histidine at different times. The p*I* of histidine is 7.61. (b) Conductivity distribution along the channel at 0, 5, 10, 20, 30, 60 min. (c) Immobilized pH profile established by stationary CACO and Tris. The pH shape maintains (almost) the same sigmoidal pattern during separation due to zero mobility of the CACO and Tris.

tions, ten ampholytes are used in a 1 cm-long channel with pH range of 6.21–8.3. Our numerical results in a 2-D planar channel agree with Svensson's results for a stepwise pH gradient.

The simulated proteins behave in a fashion similar to the ampholytes except that, since the initial number of moles of protein is substantially smaller than that of the ampholytes, they focus to a near-Gaussian peak rather than to a plateau (see Fig. 5). The proteins migrate toward the center of the channel from the edges, forming twin peaks at opposite ends of the channel which sweep toward their p*I*s from both sides. This phenomenon results from their higher charges and, hence, electrophoretic mobilities when they are exposed to a pH further away from their p*I*. These protein peaks continue to move into the interior of the channel until a single focused band forms at $x = 0.5$ cm. However, the final protein concentration is more than 80 times its initial concentration, while the concentration factor in ampholytes is less than 10 mainly due to the difference between the protein and ampholyte initial concentrations. To a first approximation, all of the amphoteric species in the channel would focus near their p*I* and at about the same concentration. At their final, focused steady state, the ampholytes occupy nearly equal volumes of the 2-D channel at nearly identical plateau concentrations but the proteins, which are initially present in smaller amounts, occupy smaller volumes and have an

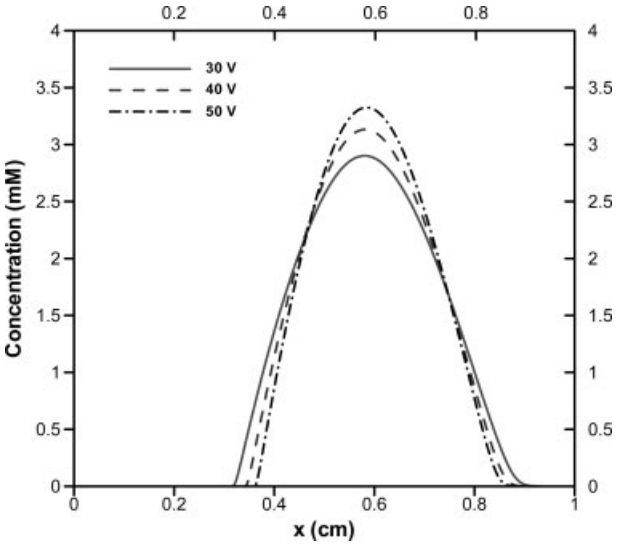

Figure 4. Effects of anodic voltage on the concentration of histidine. Anodic voltages are varied between 30 and 50 V, while the cathode is connected to the ground. Numerical results are extracted at the channel centerline (along *AA′* line in Fig. 1a) at 60 min.

insufficient mass to focus to the plateau concentration. If more protein was added to this simulation, its peak concentration would increase until it reached the same concentration as the ampholytes. This behavior is identical to the results found in published studies where a 1-D model has been used to simulate IEF in an ampholyte-based pH gradient [12].

Figure 7 shows the effect of voltage on the focusing speed: the focusing time is inversely proportional to the applied electric field. That is, the focusing time of a protein is decreased three-fold when the applied electric potential at anode is changed from 100 to 300 V. Numerical results also show that, for a particular configuration, a higher electric potential is capable of forming a tighter band within a specific time interval.

5.3 IEF by ampholyte-based pH gradient in a contraction–expansion channel

To simulate the behavior of proteins and ampholytes in a complex 2-D geometry during focusing, a 3:1:3 gradual contraction–expansion channel is chosen as illustrated in Fig. 1b. The pH gradient was formed using 20 ampholytes with four proteins focusing within the pH range, 6.21–8.3. Here, the channel width on the anodic side before the contraction region, and the cathodic side after the expansion region is 1.5 mm, the width of the throat region is 0.5 mm, and the total channel length is 1 cm. The oblique angles connecting the expanded and contracted sections are set at 30° and the input parameters for this simulation are given in Table 3. The ΔpIs of the carrier ampholytes are equally spaced as was

Table 3. Input properties of 20 ampholytes and 4 proteins used for IEF simulation in a 2-D contraction–expansion channel

Component	pK_1	pK_2	pI	Concentration (mol/m^3)	Mobility (m^2/V·s)
Ampholyte 1	6.11	6.31	6.21	0.16	3.0E-08
Ampholyte 2	6.22	6.42	6.32	0.16	3.0E-08
Ampholyte 3	6.33	6.53	6.43	0.16	3.0E-08
Ampholyte 4	6.44	6.64	6.54	0.16	3.0E-08
Ampholyte 5	6.55	6.75	6.65	0.16	3.0E-08
Ampholyte 6	6.66	6.86	6.76	0.16	3.0E-08
Ampholyte 7	6.77	6.97	6.87	0.16	3.0E-08
Ampholyte 8	6.88	7.08	6.98	0.16	3.0E-08
Ampholyte 9	6.99	7.19	7.09	0.16	3.0E-08
Ampholyte 10	7.10	7.30	7.20	0.16	3.0E-08
Ampholyte 11	7.21	7.41	7.31	0.16	3.0E-08
Ampholyte 12	7.32	7.52	7.42	0.16	3.0E-08
Ampholyte 13	7.43	7.63	7.53	0.16	3.0E-08
Ampholyte 14	7.54	7.74	7.64	0.16	3.0E-08
Ampholyte 15	7.65	7.85	7.75	0.16	3.0E-08
Ampholyte 16	7.76	7.96	7.86	0.16	3.0E-08
Ampholyte 17	7.87	8.07	7.97	0.16	3.0E-08
Ampholyte 18	7.98	8.18	8.08	0.16	3.0E-08
Ampholyte 19	8.09	8.29	8.19	0.16	3.0E-08
Ampholyte 20	8.20	8.40	8.30	0.16	3.0E-08
Protein 1	6.40	6.60	6.50	0.016	3.0E-08
Protein 2	6.94	7.14	7.04	0.016	3.0E-08
Protein 3	7.40	7.60	7.50	0.016	3.0E-08
Protein 4	7.90	8.10	8.00	0.016	3.0E-08

the case with the simple rectangular geometry and the initial concentration of each ampholyte is ten times that of each protein. A potential of 100 V is imposed at the anode and 0 V (ground) at the cathode.

Figure 8 presents the concentration distribution of proteins and ampholytes in a contraction–expansion channel at different times. The ampholytes initially behave in a fashion similar to the simple rectangular channel when an electric field is applied. However, in this case all the ampholytes in the contracted throat region ($0.25<x<0.75$ cm) have focused to broad plateaus, while the ampholytes in the two expanded regions are focused into narrow bands (Fig. 8). This phenomenon occurs because each of the ampholytes is present at the same molar loading and, after focusing, would like to occupy equal volumes of the channel at approximately identical concentrations. However, since the throat region has a smaller cross-section, those ampholytes that focus in this section must occupy a greater length of the channel resulting in a so-called "ZOOM" effect where the ampholytes in the throat region stretch out. Note that a 1-D (numerical) model cannot simulate this kind of behavior.

At steady state, the concentrations of all ampholytes are almost the same, except for those with pK values close to protein's pI (Fig. 8d). For example, the concentrations of ampholytes 10 and 11 are 3.27 mM, while the concentrations of ampholytes 3 and 4 are 3.11 and 3.16 mM, respectively,

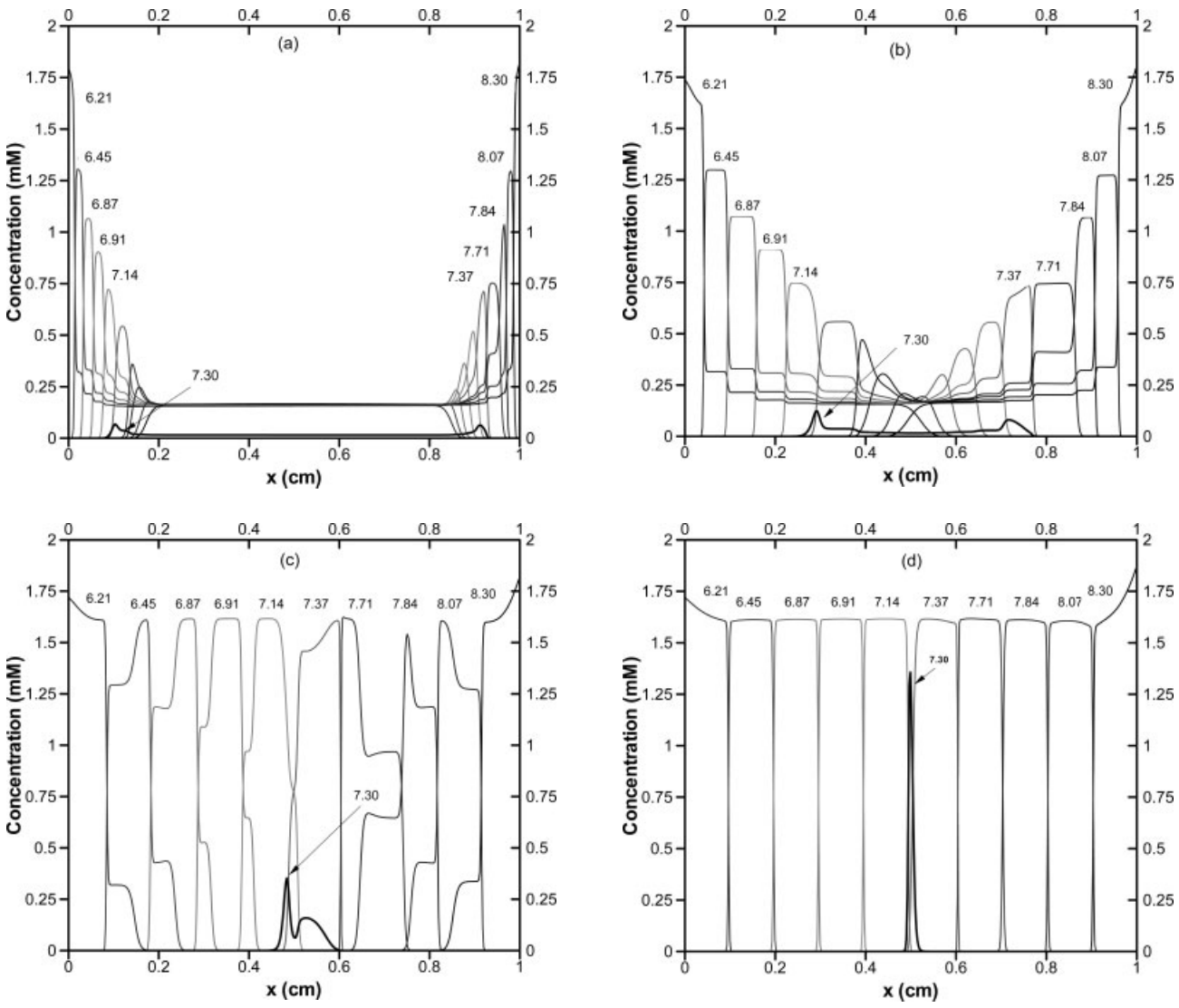

Figure 5. Concentration distributions of ten ampholytes and one protein used in ampholyte-based pH gradient IEF in a 2-D planar microchannel at (a) 3 s, (b) 10 s, (c) 25 s, and (d) 80 s. Numerical results are extracted at the channel centerline (along *AA′* line in Fig. 1a). The potentials at the anodic and cathodic side are 300 and 0 V, respectively.

due to the presence of protein 1. The main reason for this is that the broad band width of protein 1 displaces the ampholyte sufficiently to reduce its height.

Our numerical results also show that proteins with p*I*s in the throat region are more tightly focused than proteins in the expanded regions (Fig. 8). To explain this, the ratio of the peak heights (concentrations) of proteins is presented in Section 3 (Eq. 27) for a contraction–expansion channel. The theoretical calculation predicts that, for a 3:1:3 contraction–expansion channel, the peak height in the throat region protein should be three times higher than that of proteins in the anodic or cathodic side expansions. However, our numerical model predicts that the peak height of a protein in the throat region should be five- to six-fold higher than a protein focused in the expanded region. This discrepancy between the theoretical and numerical peak height value occurs because the molar concentration of proteins in the throat region starts far below the concentration of ampholytes and attempts to reach the same height as the ampholytes due to the higher electric field in the throat as compared with the contraction–expansion region. In addition, our theoretical model is based on a linear system, but the numerical solution is obtained using a highly nonlinear system.

In the 3:1:3 contraction–expansion channel simulation, the resolution of proteins 2 and 3 in the throat was found to be 13.9 at 110 s (Fig. 8d) for a nominal electric field strength of 100 V/cm. This resolution is much higher than that of the same protein/ampholyte system in a straight channel where

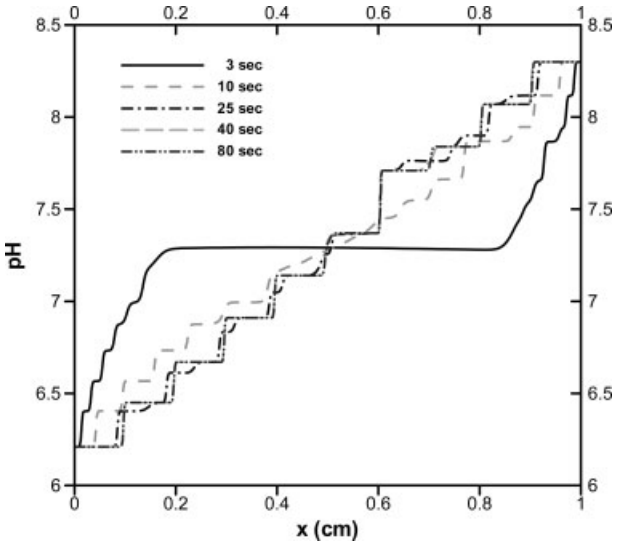

Figure 6. pH profiles evolution in a 2-D planar microchannel for ampholyte-based pH gradient IEF. These pH profiles are based on results presented in Fig. 5.

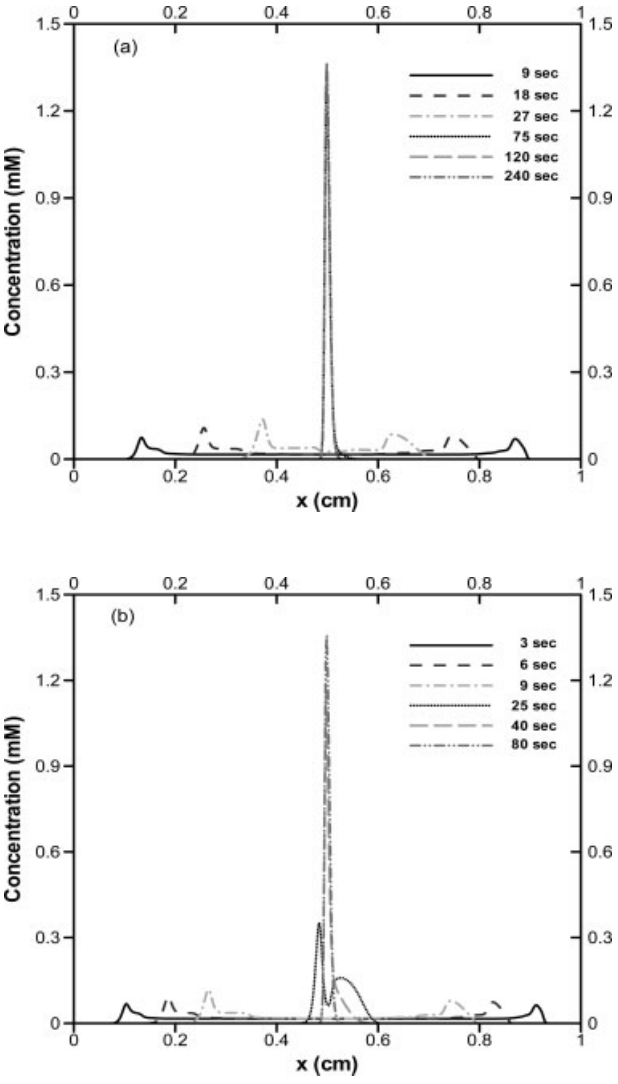

Figure 7. Transient behavior of protein in a 2-D planar microchannel at different electric potentials; (a) and (b) are simulated for anodic potentials of 100 and 300 V, respectively, while the cathodic potential was 0 V. Like Fig. 5, protein concentrations are obtained along the channel centerline.

the theoretical resolution based on Eq. (24) would be 2.9 for the same nominal electric field. There are two basic reasons for this increase. First, assuming the conductivity is uniform throughout the channel, the current density and therefore the electric field strength are greater by a factor of 3 in the throat of the channel. Second, assuming that each of our ampholytes will occupy the same fraction of the channel volume regardless of its shape, we see that the ampholyte gradient in the straight channel is just under half that in the throat region of the contraction–expansion channel. Therefore, using Eq. (24) we would expect an increase in resolution of about $\sqrt{3 \times 2} \cong 2.44$ rather than 4.8 found here. The reasons for the discrepancy in the increase in resolution are not currently known but could be an artifact of the finite number of ampholytes used in this simulation.

Figure 9 shows the pH profiles for a 2-D contraction–expansion channel. In this case, three distinct regions are apparent in the pH profile: a steep pH gradient in both the anodic and cathodic expanded regions and a shallow, high-resolution gradient in the throat region. In the throat region, the pH gradient is shallow because the band width of the ampholytes is wider than it is in the expanded regions (Fig. 8d) where the pH gradient is ~2.4 times steeper than that of throat region. Moreover, the pH profile is stepwise in the throat region due to the presence of only six ampholytes between 0.25 and 0.75 cm. The stepwise pH profile in the throat is similar to the profile in a 2-D planar channel where pH gradient is formed in the presence of ten ampholytes in a 1 cm long microchannel (Fig. 6).

The 2-D transient behavior of focusing proteins is shown in Fig. 9 for both straight and contraction–expansion channels. In a 2-D planar microchannel, the edges of the protein band remain straight (Fig. 10a) during the entire separation process. However, in a contraction–expansion channel, the protein band deforms to an arched shape while passing through the trapezoidal reducing region. This change in band shape arises from bending of the current streamlines as they pass through the trapezoidal reduction. Since solutes in the center of the channel travel a shorter distance as they pass through this region, they arrive in the throat region slightly ahead of solutes near the wall. It is important to note that the edges of the protein bands remain straight in the uniform cross-sectional region (close to the cathodic and anodic sides) but take on a crescent shape in the expansion and contraction regions. Moreover, the distorted protein band recovers from the crescent distortion in the interior of the throat region where the electric field is uniform.

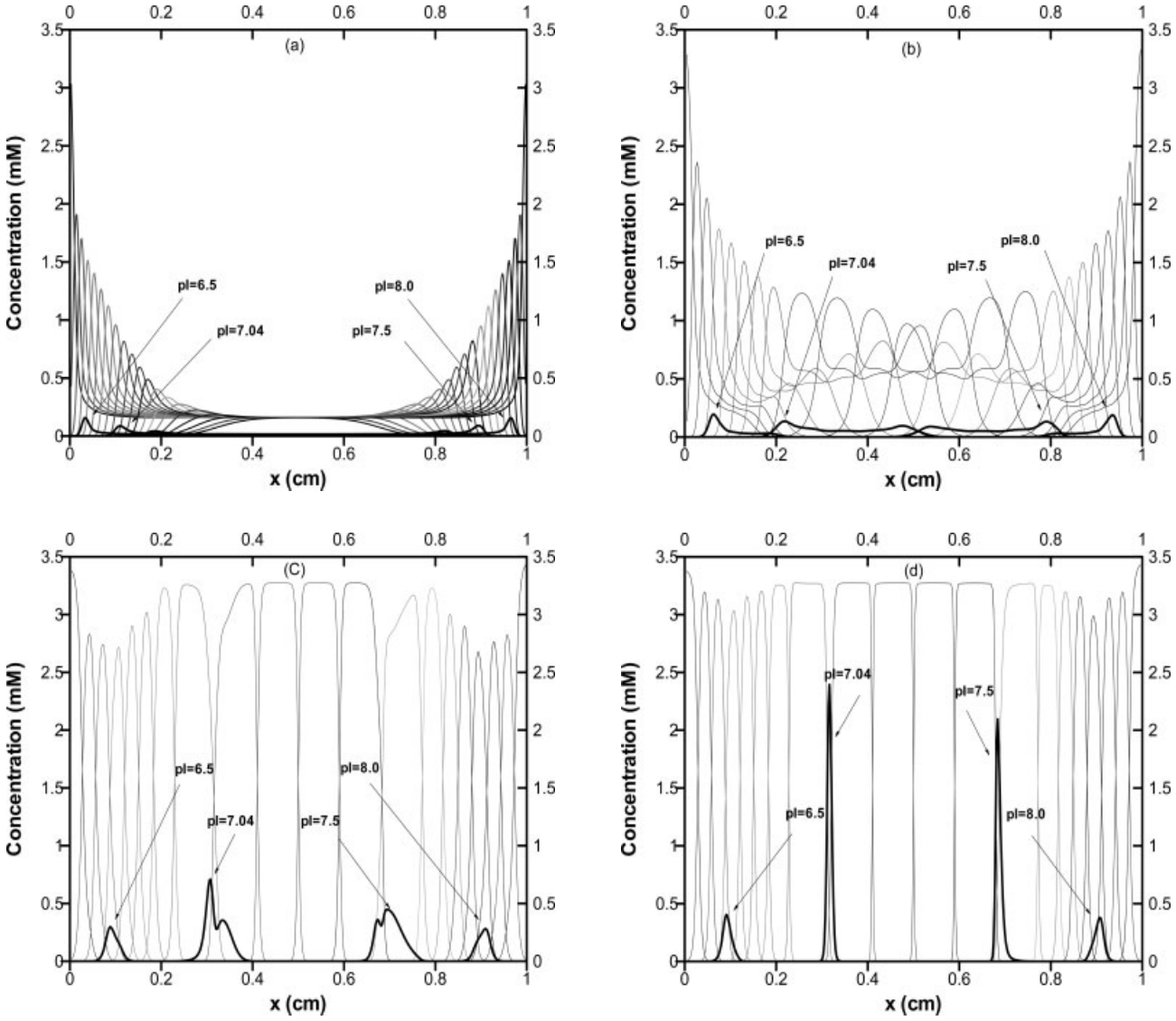

Figure 8. Concentration distributions of 20 ampholytes and 4 proteins used in ampholyte-based pH gradient IEF in a 2-D contraction–expansion microchannel at (a) 20 s, (b) 40 s, (c) 65 s, and (d) 110 s. Numerical results are extracted at the channel centerline (along *AA′* line in Fig. 1b). The potentials at the anodic and cathodic side are 100 and 0 V, respectively.

Figure 11 illustrates how four proteins with p*I*s = 6.50, 7.04, 7.50, and 8.00 are focused in a contraction-expansion channel in the presence of 20 ampholytes with two proteins in the throat region and two in the expanded region. Starting from an initially homogeneous mixture, in every case the proteins form a pair of waves which move in from either side of the channel until they merge at their respective p*I*s. Two important features are immediately apparent in this figure: First, the proteins in the throat region focus to a noticeably higher concentration than those in the expansion region and with a somewhat thinner base, implying higher peak capacities and resolution in this region. Second, with an applied voltage of 100 V across a 1 cm channel, the focusing time is less than 90 s.

6 Concluding remarks

A generalized 2-D IEF model is presented which simulates the simultaneous IEF of ampholytes and proteins in a microchip under a constant applied electric potential at electrode reservoirs. Our model is based on the equations of mass conservation, charge conservation, and includes the ionic dissociation relations which allow the amphoteric compounds to vary their charge state while they self-focus under the action of an applied field. To check this model against previously published 1-D work [12], 2-D IPG IEF is performed in the presence of stationary CACO and Tris with histidine as a mobile component. The results of this simulation agree qualitatively with the calculations reported in [12].

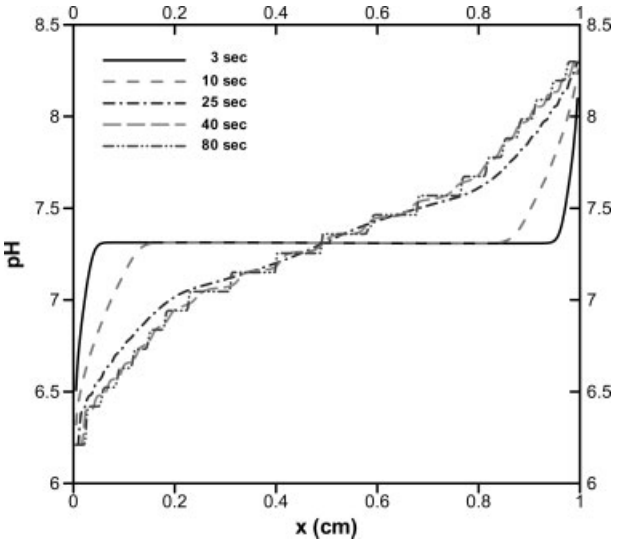

Figure 9. pH profiles evolution in a 2-D contraction–expansion microchannel for natural pH gradient IEF. These pH profiles are based on results presented in Fig. 8.

It should be noted that our simulation results are based on a constant applied potential while a constant current density was used in the work of Palusinski *et al.* [12], and so identical results were not expected. In immobilized IEF, the effect of anodic and cathodic voltages on the rate at which histidine focuses was also studied. Numerical results show that the focusing time decreases with the applied electric potential.

Simulations of ampholyte-based IEF were also presented for two different geometries: a 2-D planar channel and a 2-D contraction–expansion channel. In the planar channel, the pH gradient is formed in the presence of ten ampholytes, and one protein is allowed to focus under several different applied electric potentials. The simulation data reveal that an ampholyte peak forms at each edge of the channel and moves toward that ampholyte's p*I* under an electric field. In the presence of ten carrier ampholytes, a stepwise pH profile, $6.21<pH<8.3$, is formed in a 1 cm channel. As the pH gradient forms, the concentration of the protein evolves to 80 times its initial concentration in less than 90 s at an applied voltage of 100 V. As was the case with the IPG, the protein is focused faster at a higher electric potential.

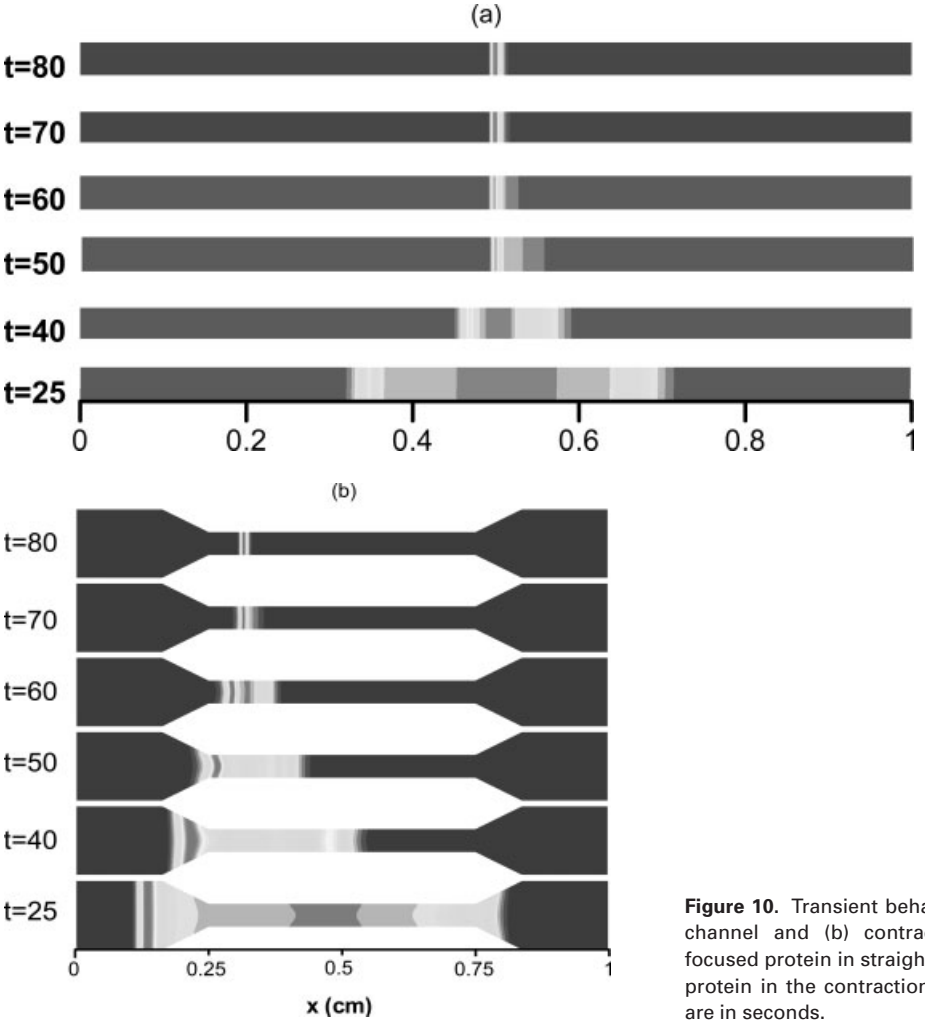

Figure 10. Transient behavior of the proteins in 2-D (a) straight channel and (b) contraction–expansion channel. The p*I* of focused protein in straight channel is 7.3, while the p*I* of focused protein in the contraction–expansion channel is 7.04. All times are in seconds.

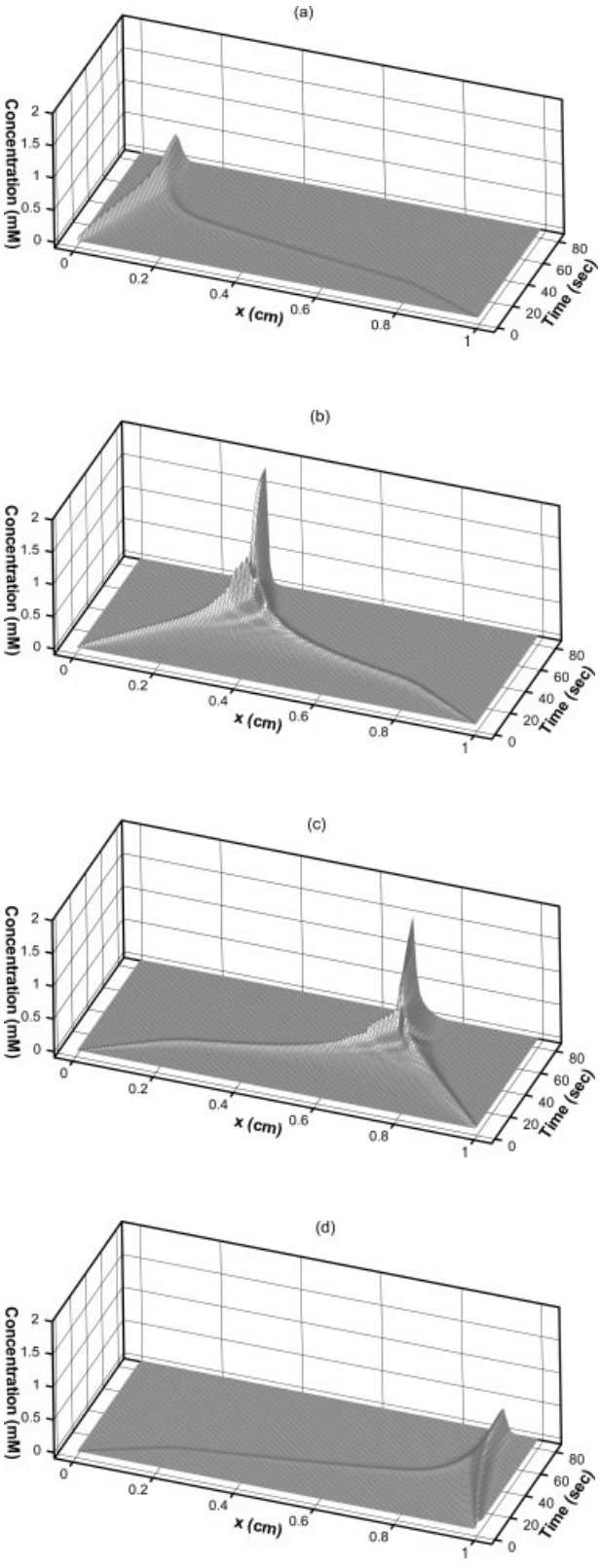

Figure 11. Transient behavior of proteins for values of p*I* (a) 6.5, (b) 7.04, (c) 7.5, and (d) 8.0. All conditions are the same as in Fig. 8.

In the contraction–expansion channel simulation, 20 ampholytes were used to form a pH gradient and four proteins were focused at a nominal electric field of 100 V/cm. In this case, ampholytes in the throat area ($0.25<x<0.75$ cm) are highly resolved, while the ampholytes in the contraction and expansion sides are more poorly focused. The protein in the throat region is focused more tightly than those on the anodic and cathodic sides due to the shallower pH gradient and the higher electric field. In a 2-D planar channel, the edges of the protein band remain uniform throughout the focusing process, while in the contraction–expansion channel, the protein band distorts to a crescent shape as it passes through the trapezoidal region. These distorted protein bands refocus in the interior of the throat region or the expanded region.

These simulations predict that resolution of low-abundance proteins can be significantly improved by mobilizing them through a contraction where the increased current density and shallow pH gradient would increase their concentration and their resolution by factors that are directly related to the relative cross-sectional areas of the throat and expansion regions.

This work was supported in part by the Washington State University Office of Research and in part by the National Science Foundation under Grant No. CTS0300802.

7 References

[1] Reuss, F. F., *Memoires de la Société Imperiale de Naturalistes de Moscou* 1809, *2*, 327.

[2] Thormann, W., Huang, T., Pawliszyn, J., Mosher, R. A., *Electrophoresis* 2004, *25*, 324–337.

[3] Chatterjee, A., *J. Micromech. Microeng.* 2003, *13*, 758–767.

[4] Mao, Q., Pawliszyn, J., Thormann, W., *Anal. Chem.* 2000, *72*, 5493–5502.

[5] Mosher, R. A., Saville, D. A., Thormann, W., *The Dynamics of Electrophoresis*, VCH, Weinheim 1992.

[6] Arnaud, I. L., Josserand, J., Rossier, J. S., Girault, H. H., *Electrophoresis* 2002, *23*, 3253–3261.

[7] Luner, S. J., Kolin, A., *Proc. Natl. Acad. Sci. USA* 1970, *66*, 898–903.

[8] Rilbe, H. Ann., *N. Y. Acad. Sci.* 1973, *209*, 11–22.

[9] Palusinski, O. A., Allgyer, T. T., Mosher, R. A., Bier, M., *Biophys. Chem.* 1981, *13*, 193–202.

[10] Bier, M., Palusinski, O. A., Mosher, R. A., Saville, D. A., *Science* 1983, *219*, 2181–2187.

[11] Saville, D. A., Palusinski, O. A., *AIChE J.* 1986, *32*, 207–214.

[12] Palusinski, O. A., Graham, A., Mosher, R. A., Bier, M., Saville, D. A., *AIChE J.* 1986, *32*, 215–223.

[13] Hoffmann, P., Ji, H., Moritz, R. L., Connolly, L. M. *et al.*, *Proteomics* 2001, *1*, 807–818.

[14] Leenov, D., Kolin, A., *J. Chem. Phys.* 1954, *22*, 683–688.

[15] Kolin, A., *J. Chem. Phys.* 1954, *22*, 1628–1629.

[16] Svensson, H., *Acta Chem. Scan.* 1961, *15*, 325–341.

[17] Cui, H., Horiuchi, K., Dutta, P., Ivory, C. F., *Anal. Chem.* 2005, *77*, 1303–1309.

[18] Cui, H., Horiuchi, K., Dutta, P., Ivory, C. F., *Anal. Chem.* 2005, *77*, 7878–7886.

[19] Štědrý, M., Jaros, M., Gaš, B., *J. Chromatogr. A* 2002, *960*, 187–198.

[20] Sounart, T. L., Safier, P. A., Baygents, J. C., in: David, G., Satinder, A. (Eds.), *Handbook of Isoelectric Focusing and Proteomics,* Elsevier, Amsterdam 2005, pp. 40–67.

[21] Righetti, P. G., *Isoelectric Focusing: Theory, Methodology and Applications*, Elsevier Biomedical Press, Amsterdam 1983.

[22] Partankar, S. V., *Numerical Heat Transfer and Fluid Flow*, Hemisphere Publishing Corp., New York 1980.

[23] Svensson, H., *J. Chromatogr.* 1966, *25*, 266–273.

